

Over-the-Air Federated Multi-Task Learning via Model Sparsification and Turbo Compressed Sensing

Haoming Ma, Xiaojun Yuan, *Senior Member, IEEE*, Zhi Ding, *Fellow, IEEE*, Dian Fan, Jun Fang, *Senior Member, IEEE*

Abstract—To achieve communication-efficient federated multi-task learning (FMTL), we propose an over-the-air FMTL (OA-FMTL) framework, where multiple learning tasks deployed on edge devices share a non-orthogonal fading channel under the coordination of an edge server (ES). In OA-FMTL, the local updates of edge devices are sparsified, compressed, and then sent over the uplink channel in a superimposed fashion. The ES employs over-the-air computation in the presence of inter-task interference. More specifically, the model aggregations of all the tasks are reconstructed from the channel observations concurrently, based on a modified version of the turbo compressed sensing (Turbo-CS) algorithm (named as M-Turbo-CS). We analyze the performance of the proposed OA-FMTL framework together with the M-Turbo-CS algorithm. Furthermore, based on the analysis, we formulate a communication-learning optimization problem to improve the system performance by adjusting the power allocation among the tasks at the edge devices. Numerical simulations show that our proposed OA-FMTL effectively suppresses the inter-task interference, and achieves a learning performance comparable to its counterpart with orthogonal multi-task transmission. It is also shown that the proposed inter-task power allocation optimization algorithm substantially reduces the overall communication overhead by appropriately adjusting the power allocation among the tasks.

Index Terms—Federated multi-task learning, over-the-air computation, turbo compressed sensing.

I. INTRODUCTION

WITH the availability of a massive amount of data at mobile edge devices, there is a growing interest in providing artificial intelligence (AI) services, such as computer vision [1] and natural language processing [2], at the edge of wireless networks. To utilize these data, conventional machine learning (ML) requires edge devices to upload their local data to a central node for model training. However, uploading such a huge volume of data by wireless communication incurs a huge cost of communication resources and compromises data privacy. To address these issues, federated learning (FL) has emerged as a popular framework for model training in a distributive and confidential manner [3]. In the FL framework, each edge device trains its local model based on its local data;

and then transmits its local model parameters or gradients to an edge server (ES). The ES updates its global model parameters via model aggregation; and then broadcasts the updated global model to the edge devices. Compared with centralized learning, FL significantly relieves the communication burden and reduces the risk of data breaches.

In federated edge learning, a huge amount of model parameters need to be uploaded from massive distributed edge devices to the ES (referred to as uplink), where limited uplink channel resources (e.g., bandwidth, time, and space) become a critical bottleneck of efficient communication. To achieve communication-efficient FL, extensive research effort has been devoted to the uplink communication design [4]–[11]. The authors in [5], [6] pointed out that the local model parameters or gradients can be sparsified, compressed, and quantized before transmission to reduce the uplink communication cost without causing substantial losses in model accuracy. The authors in [7], [8] proposed further improvements to reduce the number of communication rounds required for convergence. Different from digital model uploading in [5]–[8], another popular uplink transmission strategy called over-the-air computation has emerged to support analog model uploading from massive edge devices [9]. Instead of orthogonal resource allocation among the devices to avoid interference, over-the-air computation allows the devices to share radio resources in model uploading by leveraging the signal-superposition property of analog transmission to conduct model aggregation over the air. To name a few, the authors in [10], [11] proposed gradient sparsification and compression prior to over-the-air transmission, where the model aggregation is reconstructed at ES via compressed sensing methods.

Besides, the distributive data among edge devices are typically neither independent nor identically distributed. This causes a major challenge called the statistical heterogeneity problem, which reduces the learning performance [12]. To address this problem, the authors in [13] proposed the federated multi-task learning (FMTL) framework to implement multiple machine learning tasks over the FL communication network, motivated by the multi-task learning frameworks [14], [15]. Empirical results demonstrate that FMTL can significantly improve the generalizability of the trained models in the presence of statistical heterogeneity, where the knowledge contained in one task can be leveraged in training the models of the other tasks. Different from the method in [13] only supporting a linear model or a linear combination of pre-trained models,

H. Ma, X. Yuan, D. Fan and J. Fang are with the National Key Laboratory of Science and Technology on Communication, the University of Electronic Science and Technology of China, Chengdu, China (e-mail: hmama@std.uestc.edu.cn; xjyuan@uestc.edu.cn; df@std.uestc.edu.cn; junfang@uestc.edu.cn). Z. Ding is with the Department of Electrical and Computer Engineering, University of California at Davis, Davis, CA 95616 USA (e-mail: zding@ucdavis.edu). The corresponding author is Xiaojun Yuan.

the authors in [16]–[18] proposed other FMTL approaches to train more general non-convex learning models such as deep neural networks. To reduce the communication overhead, over-the-air computation is still an appealing solution to the uplink communication design of FMTL. Yet, the inter-task interference arises due to the concurrent transmissions of the model updates of multiple tasks. The inter-task interference, if not appropriately handled, will incur significant model aggregation errors that seriously degrade the learning performance.

To address the above challenge, in this paper, we propose the over-the-air FMTL (OA-FMTL) framework to achieve communication-efficient FMTL in the presence of inter-task interference, where multiple learning tasks are deployed on edge devices and a single ES. The ES is dedicated to parameter learning of multiple tasks, and the model aggregations of all the tasks are concurrently conducted at the ES via over-the-air computation. More specifically, at each edge device, the local model updates of all tasks are first sparsified and compressed individually by following the approach in [5], [7], and then superimposed and sent over the uplink channel. At the ES, the model aggregations of all the tasks are reconstructed from the channel observation data, based on a modified version of the turbo compressed sensing (Turbo-CS) algorithm [19] (named as M-Turbo-CS). It is clear that the above non-orthogonal transmission of multi-task model updates reduces the required uplink communication resource, but at the cost of severe inter-task interference. We show that our proposed OA-FMTL framework with M-Turbo-CS is able to efficiently suppress the inter-task interference, thereby significantly reducing the communication overhead, as compared to its counterpart with orthogonal multi-task transmission.

We further analyze the performance of the proposed OA-FMTL framework together with the M-Turbo-CS algorithm. Specially, we establish the state evolution to characterize the behaviour of the M-Turbo-CS algorithm. We then develop an upper bound on the learning loss of the OA-FMTL framework by taking model aggregation errors introduced by model sparsification, model misalignment, as well as imperfect reconstruction by M-Turbo-CS, into account. Based on that, we formulate a communication-learning optimization problem to improve the system performance by adjusting the power allocation among multiple tasks on the edge devices. We show that, under mild conditions, the problem can be solved by a feasibility test together with bisection search.

Numerical simulations show that our proposed OA-FMTL effectively suppresses the inter-task interference, so as to achieve a learning performance comparable to the single-task counterpart scheme [10], [11]. In other words, the communication overhead of OA-FMTL is only approximately one N -th of the conventional orthogonal scheme with independent training of each task, where N is the total number of tasks. Meanwhile, simulations also show that our proposed optimization algorithm further reduces the communication overhead by appropriately adjusting the power allocation among the tasks.

The remainder of this paper is organized as follows. In Section II, we describe the FMTL model and the over-the-air model aggregation framework. In Section III, we give the specific implementation of the OA-FMTL framework,

including operations at devices, operations at the ES, and the design of the M-Turbo-CS algorithm. In Section IV, we analyze the performance of OA-FMTL and formulate an optimization problem that minimizes the training loss. In Section V, we develop an effective algorithm to solve the optimization problem. In Section VI, we validate our proposed OA-FMTL framework with experiments.

Notations: Throughout, we use \mathbb{R} and \mathbb{C} to denote the real and complex number sets, respectively. Regular letters, bold small letters, and bold capital letters are used to denote scalars, vectors, and matrices, respectively. We use $(\cdot)^T$ and $(\cdot)^H$ to denote the transpose and the conjugate transpose, respectively. We use $\mathcal{CN}(\mu, \sigma^2)$ to denote the circularly-symmetric complex normal distribution with mean μ and covariance σ^2 , $\|\cdot\|$ to denote the l_2 norm, $\|\cdot\|_F$ to denote the Frobenius norm, \mathbf{I}_N to denote the $N \times N$ identity matrix, $\text{tr}(\cdot)$ to denote the trace of a square matrix, $\text{inv}(\cdot)$ to denote the inverse of a square matrix, $[k]$ to denote the integer set $\{1, \dots, k\}$, \mathbb{R}^+ to denote the set of nonnegative real numbers, \circ to denote the Hadamard product, $\mathbf{A} \succeq 0$ to denote that the matrix \mathbf{A} is positive semidefinite, $\mathbb{E}[\cdot]$ to denote the expectation operator, and $\text{var}[a|b] = \mathbb{E}[|a - \mathbb{E}[a|b]|^2|b]$.

II. SYSTEM MODEL

A. Federated Multi-Task Learning

We consider an FMTL system with N learning tasks deployed on M wireless local devices with the help of an ES, where task assignment to the devices is flexibly determined according to the computation power and storage capability of each device, as depicted in Fig. 1. Each task n on device m is associated with its local dataset D_{nm} . Following [13], [16], [20], the FMTL problem is defined as

$$\min_{\Theta, \Omega} \mathcal{L}(\Theta) + \kappa_1 \text{tr}(\Theta\Theta^T) + \kappa_2 \text{tr}(\Theta\Omega^{-1}\Theta^T) \quad (1a)$$

$$s.t. \quad \Omega \succeq 0, \quad (1b)$$

$$\text{tr}(\Omega) = 1, \quad (1c)$$

where $\Theta = [\theta_1, \dots, \theta_N] \in \mathbb{R}^{d \times N}$ models the parameters of the N tasks with θ_n being the parameter vector of task n and d being the common length of the model parameter vectors of all the tasks; $\Omega \in \mathbb{R}^{N \times N}$ models the correlation between the N tasks and is initialized to $\frac{1}{N}\mathbf{I}_N$; and κ_1, κ_2 are both the regularization parameters. In (1a), the first term is the empirical learning loss defined as

$$\mathcal{L}(\Theta) = \sum_{n=1}^N \mathcal{L}_n(\theta_n), \quad (2)$$

where $\mathcal{L}_n(\theta_n)$ is the empirical learning loss of each task n , defined by

$$\mathcal{L}_n(\theta_n) = \sum_{m=1}^M \mathcal{L}_{nm}(\theta_n); \quad (3)$$

the local empirical loss function of task n on device m is defined by

$$\mathcal{L}_{nm}(\theta_n) = \sum_{k=1}^{K_{nm}} l_n(\theta_n; \mathbf{u}_{nmk}), \quad (4)$$

where $l_n(\theta_n; \mathbf{u}_{nmk})$ is the sample-wise loss function specified by task n , \mathbf{u}_{nmk} denotes the k -th local data sample of dataset D_{nm} , and K_{nm} is the cardinality of D_{nm} with $K_{nm} = 0$ meaning that D_{nm} is empty. The second term of (1a) penalizes the complexity of Θ , and the third term measures the relationships between all tasks based on Θ and Ω [20]. The constraint (1b) is due to the fact that Ω is defined as the task covariance matrix [20], and the constraint (1c) is to restrict the complexity of Ω .

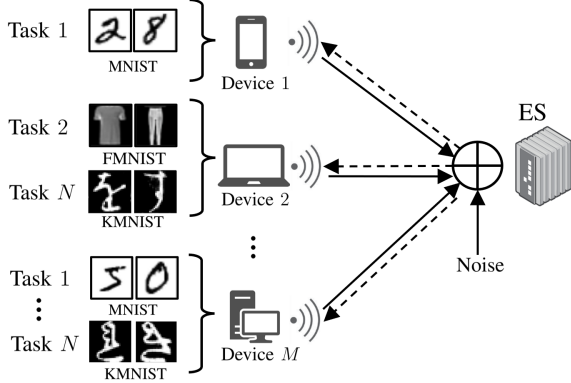


Fig. 1. An illustration of the FMTL framework.

The minimization of (1) is typically solved by the alternating descent method (ADM) [20] in the FMTL framework over a wireless communication network. Specifically, at each communication round t , each device m firstly uploads local gradients $\{\mathbf{g}_{nm}^{(t)}\}_{n=1}^N$ to the ES over a wireless uplink with $\mathbf{g}_{nm}^{(t)} = \nabla_n \mathcal{L}_{nm}(\theta_n^{(t)}) \in \mathbb{R}^d$ denoting the local gradient of task n at device m , where $\nabla_n = \frac{\partial}{\partial \theta_n} \in \mathbb{R}^d$ is the gradient operator with respect to θ_n . Then the ES optimizes the FMTL problem (1) with respect to Θ through a gradient-based update for a fixed Ω , i.e., the global model parameter Θ is updated via

$$\Theta^{(t+1)} = \Theta^{(t)} - \eta \left(\left[\sum_{m=1}^M \mathbf{g}_{1m}^{(t)}, \dots, \sum_{m=1}^M \mathbf{g}_{Nm}^{(t)} \right] + \kappa_1 \Theta^{(t)} + \kappa_2 \Theta^{(t)} \Omega^{(t)-1} \right), \quad (5)$$

where η is a predetermined learning rate. With the definition of gradients $\mathbf{g}_{nm}^{(t)}$, (5) is equivalently rewritten as

$$\Theta^{(t+1)} = \Theta^{(t)} - \eta \left(\nabla \mathcal{L}(\Theta^{(t)}) + \kappa_1 \Theta^{(t)} + \kappa_2 \Theta^{(t)} \Omega^{(t)-1} \right), \quad (6)$$

where $\nabla = \frac{\partial}{\partial \Theta} \in \mathbb{R}^{d \times N}$ is the gradient operator with respect to Θ . Since the FMTL problem (1) is convex with respect to Ω for a fixed Θ [20], the ES updates the matrix Ω via

$$\Omega^{(t+1)} = \frac{\left(\Theta^{(t+1)T} \Theta^{(t+1)} \right)^{\frac{1}{2}}}{\text{tr} \left(\left(\Theta^{(t+1)T} \Theta^{(t+1)} \right)^{\frac{1}{2}} \right)}. \quad (7)$$

After that, $\Theta^{(t+1)}$ is broadcast to all the devices by the ES over a wireless downlink to synchronize the learning models among the devices. The iterative process in (6)-(7) continues until the learning tasks converge.

B. Over-the-Air Channel Model

We now describe the wireless channels used to support the above FMTL process. It is well known that the communication bottleneck of FL resides in the uplink gradient aggregation. Thus, following the convention in [10], [11], [21], we assume error-free transmission in the downlink; and focus on the system design for the uplink. We model the wireless uplink as a block-fading multiple access (MAC) channel, where the channel state information (CSI) remains unchanged within s channel uses. Since the update in (5) depends only on the sum of the local gradients, we employ the over-the-air computation for efficient model aggregation. Specifically, at the t -th communication round, the devices, each equipped with a signal antenna, send their signal to the ES over the block-fading MAC channel with s channel uses, characterized by

$$\mathbf{r}^{(t)} = \sum_{m=1}^M h_m^{(t)} \mathbf{x}_m^{(t)} + \mathbf{w}, \quad (8)$$

where $\mathbf{x}_m^{(t)} \in \mathbb{C}^s$ is the channel input vector from device m , $h_m^{(t)} \in \mathbb{C}$ is the channel gain from device m to the ES, $\mathbf{r}^{(t)} \in \mathbb{C}^s$ is the channel output received by the ES, and $\mathbf{w} \in \mathbb{C}^s$ is an independent additive white Gaussian noise (AWGN) with each element independent and identically distributed as $\mathcal{CN}(0, \sigma_w^2)$. The power consumption of device m at each round t is constrained by

$$\mathbb{E}[\|\mathbf{x}_{m,k}^{(t)}\|^2] \leq P_m, \quad (9)$$

where $x_{m,k}^{(t)}$ is the k -th entry of $\mathbf{x}_m^{(t)}$, and P_m is the power budget of device m .

The remaining issue is to map the gradient vectors $\{\mathbf{g}_{nm}^{(t)}\}_{n=1}^N$ to the complex vector $\mathbf{x}_m^{(t)}$ at device m in each communication round t , and to recover $\nabla \mathcal{L}(\Theta^{(t)})$ in (6) from $\mathbf{r}^{(t)}$ at the ES. As inspired by [10], [11], [19], [21], [22], we employ compressed sensing and error accumulation techniques to improve the communication efficiency. The details of the uplink transceiver design in the devices and the ES are presented in what follows.

III. PROPOSED TRANSMISSION SCHEME

A. Operations at Devices

To support the uplink transmission of the OA-FMTL framework, we process the local gradients of each task n on device m , with the gradient sparsification scheme proposed in [11] and a distinct gradient compression scheme proposed in this paper. Specifically, at each round t , device m firstly adds $\mathbf{g}_{nm}^{(t)}$ defined above (5) with the error accumulation term $\Delta_{nm}^{(t)} \in \mathbb{R}^d$ as

$$\mathbf{g}_{nm}^{\text{ac}(t)} = \mathbf{g}_{nm}^{(t)} + \Delta_{nm}^{(t)}, \forall m \in [M], \forall n \in [N], \quad (10)$$

where $\Delta_{nm}^{(t)}$ is accumulated in the previous rounds with $\Delta_{nm}^{(1)}$ initialized to $\mathbf{0}$. Then device m sets all the elements of $\mathbf{g}_{nm}^{\text{ac}(t)} \in \mathbb{R}^d$ to zero except for the k_n elements with the greatest magnitudes, defined by a mapping as

$$\mathbf{g}_{nm}^{\text{sp}(t)} = \text{sp}(\mathbf{g}_{nm}^{\text{ac}(t)}, k_n) \in \mathbb{R}^d, \forall m \in [M], \forall n \in [N]. \quad (11)$$

$\Delta_{nm}^{(t)}$ is updated by

$$\Delta_{nm}^{(t+1)} = \mathbf{g}_{nm}^{\text{ac}(t)} - \mathbf{g}_{nm}^{\text{sp}(t)}, \forall m \in [M], \forall n \in [N]. \quad (12)$$

Then $\mathbf{g}_{nm}^{\text{sp}(t)}$ is normalized to $\mathbf{g}_{nm}^{\text{no}(t)} \in \mathbb{R}^d$ by

$$\mathbf{g}_{nm}^{\text{no}(t)} = \frac{\mathbf{s}_n \circ \mathbf{g}_{nm}^{\text{sp}(t)}}{v_{nm}^{(t)}}, \quad (13)$$

where $v_{nm}^{(t)} = \frac{1}{\sqrt{d}} \|\mathbf{g}_{nm}^{\text{sp}(t)}\|$ is a normalization factor, and $\mathbf{s}_n \in \mathbb{R}^d$ is a random sign vector with the entries independently and uniformly drawn from $\{+1, -1\}$. Note that \mathbf{s}_n ensures that the entries of $\mathbf{g}_{nm}^{\text{no}(t)}$ have zero-mean, and $\mathbf{g}_{nm}^{\text{no}(t)}$ of task n is independent of the gradients of the other tasks.

Next $\mathbf{g}_{nm}^{\text{no}(t)}$ is compressed into a low-dimensional vector $\mathbf{g}_{nm}^{\text{cp}(t)} \in \mathbb{R}^{2s}$ by a compression matrix $\mathbf{A}_n \in \mathbb{R}^{2s \times d}$ as

$$\mathbf{g}_{nm}^{\text{cp}(t)} = \mathbf{A}_n \mathbf{g}_{nm}^{\text{no}(t)}, \forall m \in [M], \forall n \in [N], \quad (14)$$

where each task n is assigned with an individual compression matrix \mathbf{A}_n . Unlike the classic over-the-air FL framework [10], [11], our proposed OA-FMTL framework needs to enable the concurrent reconstruction of the gradient aggregations of the N tasks at the ES, where the randomness of the compression matrices is introduced to help eliminate the inter-task interference. In specific, we employ a partial discrete cosine transform (DCT) matrix $\mathbf{A}_n = \mathbf{S}_n \mathbf{F}$ for each task n , where the selection matrix $\mathbf{S}_n \in \mathbb{R}^{2s \times d}$ consists of $2s$ randomly selected rows of the $d \times d$ identity matrix \mathbf{I}_d and the (m, n) -th entry of the unitary DCT matrix $\mathbf{F} \in \mathbb{R}^{d \times d}$ is given by $\sqrt{\frac{2}{d}} \cos\left(\frac{(m-1)(2n-1)\pi}{2d}\right)$ when $m \neq 1$, or $\sqrt{\frac{1}{d}}$ when $m = 1$. Compared to other choices of the compression matrix such as the i.i.d. Gaussian matrix, the partial DCT matrix has advantages both in performance and complexity [23].

We are now ready to describe the design of $\mathbf{x}_m^{(t)}$. As a distinct feature of the OA-FMTL framework, we propose to superimpose the local gradients of different tasks to support the multiplexing of the N learning tasks. In specific, each device m constructs

$$\tilde{\mathbf{x}}_m^{(t)} = \sum_{n=1}^N \sqrt{\gamma_n^{(t)}} \mathbf{g}_{nm}^{\text{cp}(t)} \in \mathbb{R}^{2s}, \quad (15)$$

where $\gamma_n^{(t)} \in \mathbb{R}^+$ is the inter-task power allocation coefficient of task n . Then $\tilde{\mathbf{x}}_m^{(t)}$ is converted into a complex vector $\tilde{\mathbf{x}}_m^{(t)} \in \mathbb{C}^s$, defined as

$$\text{Re}\{\tilde{\mathbf{x}}_m^{(t)}\} = \left[\tilde{x}_{m,1}^{(t)}, \dots, \tilde{x}_{m,s}^{(t)} \right]^T, \quad (16a)$$

$$\text{Im}\{\tilde{\mathbf{x}}_m^{(t)}\} = \left[\tilde{x}_{m,s+1}^{(t)}, \dots, \tilde{x}_{m,2s}^{(t)} \right]^T, \quad (16b)$$

where $\tilde{x}_{m,k}^{(t)}$ is the k -th entry of $\tilde{\mathbf{x}}_m^{(t)}$. After that, every device m concurrently sends $\mathbf{x}_m^{(t)} = \alpha_m^{(t)} \tilde{\mathbf{x}}_m^{(t)}$ to the ES via analog transmission, where the power allocation coefficient $\alpha_m^{(t)} \in \mathbb{C}$ is given by

$$\alpha_m^{(t)} = \frac{|h_m^{(t)}|}{h_m^{(t)}} \sqrt{\frac{P_m}{2}}. \quad (17)$$

We see that the phase of $\alpha_m^{(t)}$ is opposite to the phase of $h_m^{(t)}$, and that with $\alpha_m^{(t)}$ in (17), the transmission power of

every device meets the power budget. This avoids the hard alignment of local gradients and hence improves the system performance; see, e.g., [24] for more detailed discussions.

B. Operations at ES

We now describe the receiver design of the ES. We assume that the ES knows the CSI $\{h_m^{(t)}\}_{m=1}^M$ at each round t . In practice, the CSI can be acquired by the ES via channel training. With (8), (13)-(17) and appropriate scaling, we construct the system model as

$$\mathbf{y}^{(t)} = [\mathbf{A}_1, \dots, \mathbf{A}_N] \left[\mathbf{g}_1^{(t)T}, \dots, \mathbf{g}_N^{(t)T} \right]^T + \mathbf{n}, \quad (18)$$

where $\mathbf{y}^{(t)} = \frac{[\text{Re}\{\mathbf{r}^{(t)}\}^T, \text{Im}\{\mathbf{r}^{(t)}\}^T]^T}{\sqrt{\sum_{m=1}^M |h_m^{(t)} \alpha_m^{(t)}|^2}}$, $\mathbf{n} \triangleq \frac{[\text{Re}\{\mathbf{w}\}^T, \text{Im}\{\mathbf{w}\}^T]^T}{\sqrt{\sum_{m=1}^M |h_m^{(t)} \alpha_m^{(t)}|^2}}$ follows $\mathcal{N}(0, \sigma^2)$ with $\sigma^2 \triangleq \frac{\sigma_w^2}{2 \sum_{m=1}^M |h_m^{(t)} \alpha_m^{(t)}|^2}$, and $\mathbf{g}_n^{(t)} \triangleq \frac{\sum_{m=1}^M \sqrt{\gamma_n^{(t)}} h_m^{(t)} \alpha_m^{(t)} \mathbf{g}_{nm}^{\text{no}(t)}}{\sqrt{\sum_{m=1}^M |h_m^{(t)} \alpha_m^{(t)}|^2}}$. Given $\mathbf{y}^{(t)}$, for $\forall n \in [N]$, the ES

reconstructs $\mathbf{g}_n^{(t)}$ as $\hat{\mathbf{g}}_n^{(t)}$ via the modified turbo compressed sensing algorithm detailed later in Section III-C. Then the ES computes the model updating vector $\check{\mathbf{g}}_n^{(t)} \in \mathbb{R}^d$ as

$$\check{\mathbf{g}}_n^{(t)} = \zeta_n^{(t)} \sqrt{\sum_{m=1}^M |h_m^{(t)} \alpha_m^{(t)}|^2} \mathbf{s}_n \circ \hat{\mathbf{g}}_n^{(t)} \in \mathbb{R}^d, \quad (19)$$

where $\zeta_n^{(t)} \in \mathbb{R}$ is a normalization scaling factor of task n to reduce the channel misalignment error caused by the incomplete channel reversion in (17), and the sign vector \mathbf{s}_n defined below (13) is known by the ES, e.g., via sharing the random seeds. Then, based on (6), the model update of OA-FMTL in the presence of the communication error is given by

$$\Theta^{(t+1)} = \Theta^{(t)} - \eta \left([\check{\mathbf{g}}_N^{(t)}, \dots, \check{\mathbf{g}}_1^{(t)}] + \kappa_1 \Theta^{(t)} + \kappa_2 \Theta^{(t)} \Omega^{(t)} \right), \quad (20)$$

where η is defined below (6).

C. Modified Turbo Compressed Sensing (M-Turbo-CS)

The recovery of $\{\mathbf{g}_n^{(t)}\}_{n=1}^N$ from $\mathbf{y}^{(t)}$ in (18) is a compressed sensing problem, where the compression matrix $\mathbf{A} = [\mathbf{A}_1, \dots, \mathbf{A}_N] \in \mathbb{R}^{2s \times dN}$ composed of N partial DCT matrices is partial orthogonal, i.e., $\mathbf{A} \mathbf{A}^T = \mathbf{I}_{2s}$. It is known that the Turbo-CS algorithm [19] is the state-of-the-art compressed sensing problem to handle partial-orthogonal sensing matrices. Inspired by this, we basically follow the idea of Turbo-CS to solve the compressed sensing problem involved in (18). But the difference is that, as each $\mathbf{g}_n^{(t)}$ is the gradient for a different task n , $\{\mathbf{g}_n^{(t)}\}_{n=1}^N$ generally have different *prior* distributions. With (13)-(18), we assume that the entries of $\mathbf{g}_n^{(t)}$ are independently drawn from a Bernoulli Gaussian distribution:

$$g_{n,k}^{(t)} \sim \begin{cases} 0, & \text{probability} = 1 - \lambda_n^{(t)}, \\ \mathcal{N}(0, \gamma_n^{(t)}), & \text{probability} = \lambda_n^{(t)}, \end{cases} \quad (21)$$

where $g_{n,k}^{(t)}$ is the k -th element of $\mathbf{g}_n^{(t)}$, $\lambda_n^{(t)}$ is the sparsity of $\mathbf{g}_n^{(t)}$, and $\gamma_n^{(t)}$ is the inter-task power allocation coefficient

defined in (15). The sparsity $\lambda_n^{(t)}$ in the *prior* distribution is estimated by the expectation-maximization algorithm [25]. With the above *prior* model, we modify the Turbo-CS algorithm accordingly to accommodate concurrent model aggregations of the N tasks as follows.

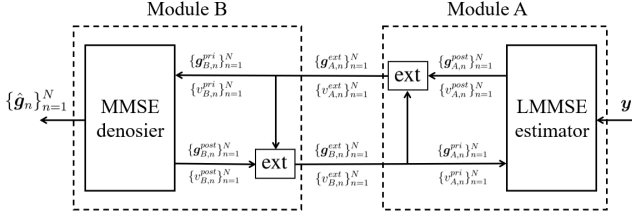


Fig. 2. An illustration of the M-Turbo-CS algorithm.

As shown in Fig. 2, M-Turbo-CS iterates between two modules where module A is a linear minimum mean-squared error (LMMSE) [26] estimator handling the linear constraint in (18), and module B is a minimum mean-squared error (MMSE) [26] denoiser exploiting the gradient sparsity in (21). The two modules are executed iteratively until convergence. For brevity, we henceforth drop out the round index t in circumstances without causing ambiguity. The detailed operations of the iterative algorithm are provided below.

The iterative process begins with Module A. Given the *prior* mean $\mathbf{g}_{A,n}^{pri} \in \mathbb{R}^d$ initialized to $\mathbf{0}$, the *prior* variance $v_{A,n}^{pri} \in \mathbb{R}^d$ initialized to 1 and the observed vector \mathbf{y} in (18) as the input of the LMMSE estimator in Module A, the *posterior* mean $\mathbf{g}_{A,n}^{post} \in \mathbb{R}^d$ and the *posterior* variance $v_{A,n}^{post} \in \mathbb{R}$ of the LMMSE estimator is given by

$$\mathbf{g}_{A,n}^{post} = \mathbf{g}_{A,n}^{pri} + \frac{\gamma_n v_{A,n}^{pri} (\mathbf{y} - \sum_{n'=1}^N \mathbf{A}_{n'} \mathbf{g}_{A,n'}^{pri})}{\sum_{n'=1}^N \gamma_{n'} v_{A,n'}^{pri} + \sigma^2} \mathbf{A}_n^T, \forall n \in [N], \quad (22a)$$

$$v_{A,n}^{post} = v_{A,n}^{pri} - \frac{s}{d} \frac{\gamma_n v_{A,n}^{pri 2}}{\sum_{n'=1}^N \gamma_{n'} v_{A,n'}^{pri} + \sigma^2}, \forall n \in [N]. \quad (22b)$$

Then Module A outputs the extrinsic message of the LMMSE estimate as

$$\mathbf{g}_{A,n}^{ext} = v_{A,n}^{ext} \left(\frac{\mathbf{g}_{A,n}^{post}}{v_{A,n}^{post}} - \frac{\mathbf{g}_{A,n}^{pri}}{v_{A,n}^{pri}} \right), \forall n \in [N], \quad (23a)$$

$$v_{A,n}^{ext} = \left(\frac{1}{v_{A,n}^{post}} - \frac{1}{v_{A,n}^{pri}} \right)^{-1}, \forall n \in [N], \quad (23b)$$

which is used to update the *prior* mean $\mathbf{g}_{B,n}^{pri} \in \mathbb{R}^d$ and the *prior* variance $v_{B,n}^{pri} \in \mathbb{R}^d$ of the MMSE denoiser in Module B as

$$\mathbf{g}_{B,n}^{pri} = \mathbf{g}_{A,n}^{ext}, \quad (24a)$$

$$v_{B,n}^{pri} = v_{A,n}^{ext}. \quad (24b)$$

For Module B, we model the *prior* mean $\mathbf{g}_{B,n}^{pri}$ as an observation of \mathbf{g}_n corrupted by additive noise \mathbf{n}_n [19]:

$$\mathbf{g}_{B,n}^{pri} = \mathbf{g}_n + \mathbf{n}_n, \quad (25)$$

where $\mathbf{n}_n \sim \mathcal{N}(0, \gamma_n v_{B,n}^{pri})$ is independent of \mathbf{g}_n . Then the *posterior* mean $\mathbf{g}_{B,n}^{post} \in \mathbb{R}^d$ and the variance $v_{B,n}^{post} \in \mathbb{R}$ of the MMSE denoiser are given by

$$\mathbf{g}_{B,n}^{post} = \mathbb{E}[\mathbf{g}_n | \mathbf{g}_{B,n}^{pri}], \forall n \in [N], \quad (26a)$$

$$v_{B,n}^{post} = \frac{1}{d\gamma_n} \sum_{k=1}^d \text{var}[g_{n,k} | \mathbf{g}_{B,n}^{pri}], \forall n \in [N], \quad (26b)$$

where $\text{var}[a|b] = \mathbb{E}[|a - \mathbb{E}[a|b]|^2 | b]$; and $g_{n,k}$ and $g_{B,n,k}^{pri}$ are the k -th elements of \mathbf{g}_n and $\mathbf{g}_{B,n}^{pri}$, respectively. Then, Module B outputs the extrinsic message of the MMSE denoiser as

$$\mathbf{g}_{B,n}^{ext} = v_{B,n}^{ext} \left(\frac{\mathbf{g}_{B,n}^{post}}{v_{B,n}^{post}} - \frac{\mathbf{g}_{B,n}^{pri}}{v_{B,n}^{pri}} \right), \forall n \in [N], \quad (27a)$$

$$v_{B,n}^{ext} = \left(\frac{1}{v_{B,n}^{post}} - \frac{1}{v_{B,n}^{pri}} \right)^{-1}, \forall n \in [N], \quad (27b)$$

which is used to update the *prior* mean $\mathbf{g}_{A,n}^{pri} \in \mathbb{R}^d$ and the variance $v_{A,n}^{pri} \in \mathbb{R}$ of the LMMSE estimator in Module A as

$$\mathbf{g}_{B,n}^{pri} = \mathbf{g}_{A,n}^{ext}, \quad (28a)$$

$$v_{B,n}^{pri} = v_{A,n}^{ext}. \quad (28b)$$

At the end of the iterative process, the final estimate of \mathbf{g}_n is based on the *posterior* output of the MMSE denoiser, i.e., $\hat{\mathbf{g}}_n = \mathbf{g}_{B,n}^{post}$.

To sum up, at each round t , given the initialization values $\mathbf{g}_{A,n}^{pri} = \mathbf{0}$ and $v_{A,n}^{pri} = 1$ defined in (21) for $\forall n \in [N]$, (22)-(24) and (26)-(28) are iterated until a certain termination criterion is met, and $\mathbf{g}_{B,n}^{post}$ is output as $\hat{\mathbf{g}}_n^{(t)}$ for the model update in (20), for $\forall n \in [N]$. Compared with the original Turbo-CS algorithm in [19], the main difference is that each subvector \mathbf{g}_n in (18) has its individual *prior* distribution as in (21). Later, we will show by performance analysis and numerical experiments in Section IV-A that the M-Turbo-CS algorithm is able to efficiently suppress the inter-task interference in model aggregation.

D. Overall Scheme

The overall scheme is summarized in Algorithm 1, where Lines 3-7 are executed at the devices, and Lines 8-19 are executed at the ES. Particularly, Line 15 of Algorithm 1 involves the optimization of this scheme, which will be elaborated later in Section V. In what follows, we present the performance analysis of the proposed scheme.

IV. PERFORMANCE ANALYSIS

A. Performance Analysis of M-Turbo-CS

To start with, we first describe the performance analysis of the M-Turbo-CS algorithm via state evolution. The main idea of state evolution is to characterize the behavior of the Turbo-CS algorithm by the variance transfer functions of the two modules [23]. Specifically, the variance transfer functions of Module A are defined by

$$z_n = \phi_n(v_1, \dots, v_N; \gamma_1, \dots, \gamma_N), \forall n \in [N], \quad (29)$$

where v_n denotes the *prior* variance of LMMSE estimator, i.e., $v_n \triangleq v_{A,n}^{pri}$, z_n denotes the reciprocal of the *prior* variance

Algorithm 1 OA-FMTL with M-Turbo-CS.

1: **Initialize** $\Delta_{nm}^{(1)} = \mathbf{0}, \Omega^{(1)} = \mathbf{I}_N, \gamma_n = \frac{1}{N}, \zeta_n = 0, \forall n \in [N], m \in [M]$
2: **for** $t = 1, 2, \dots$ **do**
3: **Each device** m **does in parallel:**
4: Compute $\{\mathbf{g}_{nm}^{(t)}\}_{n=1}^N$ with $\{D_{nm}\}_{n=1}^N$ and $\boldsymbol{\theta}^{(t)}$
5: Compute $\{\mathbf{x}_m^{(t)}\}_{n=1}^N$ via (10)-(11) and (13)-(17)
6: Compute $\{\Delta_{nm}^{(t+1)}\}_{n=1}^N$ via (12)
7: Send $\mathbf{s}_m^{(t)}$ to the ES over the channel in (8)
8: **ES does:**
9: Receive $\mathbf{r}^{(t)}$ via (8) and compute $\mathbf{y}^{(t)}$ via (18)
10: **Initialize** $\mathbf{g}_{A,n}^{pri} = \mathbf{0}, v_{A,n}^{pri} = 1, \forall n \in [N]$
11: **repeat**
12: Update $\{\mathbf{g}_{B,n}^{post}\}_{n=1}^N$, via (22)-(27)
13: **until** convergence
14: $\hat{\mathbf{g}}_n^{(t)} = \mathbf{g}_{B,n}^{post}, \forall n \in [N]$
15: Update $\{\gamma_n^{(t)}, \zeta_n^{(t)}\}_{n=1}^N$ via calling Algorithm 2
16: $\hat{\mathbf{g}}_n^{(t)} = \zeta_n^{(t)} \sqrt{\sum_{m=1}^M |h_m^{(t)} \alpha_m^{(t)}|^2} \mathbf{s}_n \circ \hat{\mathbf{g}}_n^{(t)}, \forall n \in [N]$
17: Update $\Theta^{(t)}$ via (20)
18: Update $\Omega^{(t)}$ via (7)
19: Broadcast $\Theta^{(t+1)}, \{\gamma_n^{(t+1)}\}_{n=1}^N$ to all the devices
20: **end for**

of MMSE denoiser, i.e., $z_n \triangleq \frac{1}{v_{B,n}^{pri}}$; and the function ϕ_n maps $\{v_n\}_{n=1}^N$ into z_n with the inter-task power allocation coefficients $\{\gamma_n\}_{n=1}^N$ known by the ES. With (22b), (23b) and (24b), the expressions of functions $\{\phi_n\}_{n=1}^N$ are given by

$$\begin{aligned} & \phi_n(v_1, \dots, v_N; \gamma_1, \dots, \gamma_N) \\ &= \left(\frac{d}{s\gamma_n} \left(\sum_{n'=1}^N \gamma_{n'} v_{n'} + \sigma^2 \right) - v_n \right)^{-1}, \forall n \in [N]. \end{aligned} \quad (30)$$

In addition, the variance transfer functions of Module B are defined by

$$v_n = \psi_n(z_n), \forall n \in [N], \quad (31)$$

where the function ψ_n maps z_n into v_n for each n with exploiting the *prior* information in (21). With (26b), (27b) and (28b), we obtain the expression of $\{\psi_n\}_{n=1}^N$ as

$$\psi_n(z_n) = \left(\frac{1}{\text{mmse}_n(z_n)} - z_n \right)^{-1}, \forall n \in [N], \quad (32)$$

where $\text{mmse}_n(z_n) = \frac{1}{\gamma_n} \mathbb{E}[\text{var}[\mathbf{g}_n | \mathbf{g}_n + \mathbf{n}_n]]$, $\mathbf{n}_n \sim \mathcal{N}(0, \gamma_n/z_n)$ is defined in (25) and \mathbf{g}_n is defined in (21). The variance transfer functions (29) and (31) iteratively characterize the variances $\{v_n\}_{n=1}^N$, with each v_n converging to v_n^* [23]. The fixed point $\{v_n^*\}_{n=1}^N$ tracks the normalized output MSEs of the recovery on $\{\mathbf{g}_n\}_{n=1}^N$ in the M-Turbo-CS algorithm. We will show that the analysis agrees well with simulations in Section VI.

B. Communication Error Analysis of OA-FMTL

We now analyze the communication error of the OA-FMTL framework. Based on (6) and (20), we define the overall model updating error at the t -th round as

$$\mathbf{E}^{(t)} = \nabla \mathcal{L}(\Theta^{(t)}) - [\hat{\mathbf{g}}_1^{(t)}, \dots, \hat{\mathbf{g}}_N^{(t)}] \in \mathbb{R}^{d \times N}. \quad (33)$$

We define the n -th columns of $\mathbf{E}^{(t)}$ as $\mathbf{e}_n^{(t)}$, which is also the model updating error from task n , characterized by

$$\mathbf{e}_n^{(t)} = \nabla_n \mathcal{L}_n(\boldsymbol{\theta}_n^{(t)}) - \hat{\mathbf{g}}_n^{(t)} \quad (34a)$$

$$\begin{aligned} &= \underbrace{\sum_{m=1}^M \mathbf{g}_{nm}^{(t)} - \sum_{m=1}^M \mathbf{g}_{nm}^{\text{sp}(t)}}_{\text{Sparsification error}} \\ &+ \underbrace{\sum_{m=1}^M \mathbf{g}_{nm}^{\text{sp}(t)} - \zeta_n^{(t)} \sqrt{\sum_{m=1}^M |h_m^{(t)} \alpha_m^{(t)}|^2} \mathbf{g}_n^{(t)}}_{\text{Misalignment error}} \\ &+ \underbrace{\zeta_n^{(t)} \sqrt{\sum_{m=1}^M |h_m^{(t)} \alpha_m^{(t)}|^2} (\mathbf{g}_n^{(t)} - \hat{\mathbf{g}}_n^{(t)})}_{\text{Estimation error from M-Turbo-CS}} \end{aligned} \quad (34b)$$

$$= \mathbf{e}_{n,1}^{(t)} + \mathbf{e}_{n,2}^{(t)} + \mathbf{e}_{n,3}^{(t)} \in \mathbb{R}^{d \times 1}, \quad (34c)$$

where $\mathbf{e}_{n,1}^{(t)} \in \mathbb{R}^d$ denotes the sparsification error caused by the step in (11), $\mathbf{e}_{n,2}^{(t)} \in \mathbb{R}^d$ denotes the channel misalignment error caused by the incomplete channel reversion in (17), and $\mathbf{e}_{n,3}^{(t)} \in \mathbb{R}^d$ denotes the estimation error caused by the imperfect recovery of M-Turbo-CS. We analyze the bound of $\mathbb{E}[\|\mathbf{E}^{(t)}\|^2]$ as

$$\mathbb{E}[\|\mathbf{E}^{(t)}\|_F^2] = \sum_{n=1}^N \mathbb{E}[\|\mathbf{e}_n^{(t)}\|^2], \quad (35)$$

where $\mathbb{E}[\|\mathbf{e}_n^{(t)}\|^2]$ is bounded as

$$\mathbb{E}[\|\mathbf{e}_n^{(t)}\|^2] \leq 3(\|\mathbf{e}_{n,1}^{(t)}\|^2 + \mathbb{E}[\|\mathbf{e}_{n,2}^{(t)}\|^2] + \mathbb{E}[\|\mathbf{e}_{n,3}^{(t)}\|^2]), \quad (36)$$

by using the triangle inequality and the inequality of arithmetic means. The analysis of $\|\mathbf{e}_{n,1}^{(t)}\|^2$ defined in (56) and $\mathbb{E}[\|\mathbf{e}_{n,2}^{(t)}\|^2]$ defined in (58) basically follows the process in [10] and [21], respectively, and is given in Appendix A. Besides, from the performance analysis of M-Turbo-CS in Section IV-A, M-Turbo-CS converges to the fixed point $\{v_n^*\}_{n=1}^N$ at the t -th round, for $\forall n \in [N]$. Thus, we have

$$\mathbb{E}[\|\mathbf{e}_{n,3}^{(t)}\|^2] = \sum_{m=1}^M |h_m^{(t)} \alpha_m^{(t)}|^2 \zeta_n^{(t)2} \gamma_n^{(t)} v_n^*(t). \quad (37)$$

C. Convergence Analysis

To proceed, we make assumptions by following the convention in stochastic optimization [27].

Assumption 1. $\mathcal{L}_n(\cdot)$ is strongly convex with some (positive) parameter Ω_n . That is, $\mathcal{L}_n(\mathbf{y}) \geq \mathcal{L}_n(\mathbf{x}) + (\mathbf{y} - \mathbf{x})^T \nabla_n \mathcal{L}_n(\mathbf{x}) + \frac{\Omega_n}{2} \|\mathbf{y} - \mathbf{x}\|^2, \forall \mathbf{x}, \mathbf{y} \in \mathbb{R}^d, \forall n \in [N]$.

Assumption 2. The gradient $\nabla_n \mathcal{L}_n(\cdot)$ is Lipschitz continuous with some (positive) parameter L . That is, $\|\nabla_n \mathcal{L}_n(\mathbf{x}) - \nabla_n \mathcal{L}_n(\mathbf{y})\| \leq L_n \|\mathbf{x} - \mathbf{y}\|, \forall \mathbf{x}, \mathbf{y} \in \mathbb{R}^d, \forall n \in [N]$.

Assumption 3. $\mathcal{L}_n(\cdot)$ is twice-continuously differentiable, for $\forall n \in [N]$.

Assumption 4. The gradient with respect to any training sample, denoted by $\nabla_n l_n(\boldsymbol{\theta}_n; \cdot)$, is upper bounded at $\boldsymbol{\theta}_n$ as

$$\|\nabla_n l_n(\boldsymbol{\theta}_n, \mathbf{u}_{nmk})\|^2 \leq \beta_{n,1} + \beta_{n,2} \|\nabla_n \mathcal{L}_n(\boldsymbol{\theta}_n)\|^2, \forall n \in [N]$$

for some constants $\beta_{n,1} \geq 0$ and $\beta_{n,2} > 0$.

Assumptions 1-4 lead to an upper bound on the loss function $\mathcal{L}_n(\boldsymbol{\theta}_n^{(t+1)})$ with respect to the model updating (20), as given in the following lemma.

Lemma 1. Let $\mathcal{L}_n(\cdot)$ satisfy Assumptions 1-4. At the t -th training round, with $L_n = 1/\eta$ for $\forall n$, we have

$$\begin{aligned} \mathbb{E}[\mathcal{L}_n(\boldsymbol{\theta}_n^{(t+1)})] &\leq \mathbb{E}[\mathcal{L}_n(\boldsymbol{\theta}_n^{(t)})] - \frac{1}{2L_n} \mathbb{E}[\|\nabla_n \mathcal{L}_n(\boldsymbol{\theta}_n^{(t)})\|^2] \\ &\quad + \frac{1}{2L_n} \mathbb{E}[\|e_n^{(t)}\|^2], \end{aligned} \quad (38)$$

where the Lipschitz constant L_n is defined in Assumption 2.

Proof. See [27, Lemma 2.1]. \square

We are now ready to derive an upper bound of the expected difference between the training loss and the optimal loss at round $t+1$, i.e., $\mathbb{E}[\mathcal{L}(\boldsymbol{\Theta}^{(t+1)}) - \mathcal{L}(\boldsymbol{\Theta}^{(t)})]$.

Theorem 1. With Assumptions 1-4,

$$\begin{aligned} \mathbb{E}[\mathcal{L}(\boldsymbol{\Theta}^{(t+1)}) - \mathcal{L}(\boldsymbol{\Theta}^{(t)})] &\leq \mathbb{E}[\mathcal{L}(\boldsymbol{\Theta}^{(1)}) - \mathcal{L}(\boldsymbol{\Theta}^{(*)})] (\max_n \Upsilon_n)^t \\ &\quad + \sum_{t'=1}^t (\max_n \Upsilon_n)^{t-t'} \sum_{n=1}^N C_n^{(t')}, \end{aligned} \quad (39)$$

where $(\cdot)^t$ denotes the t -th power, $\mathcal{L}(\cdot)$ is the total empirical loss function defined in (1), $\boldsymbol{\Theta}^{(1)}$ is the initial system model parameter, and the functions Υ_n , $C_n^{(t)}$ for each task n are defined as

$$\Upsilon_n \triangleq 1 - \frac{\Omega_n}{L_n} + \frac{3\Omega_n\beta_{n,2}}{L_n} \left(\frac{2r_n}{1-r_n} \right)^2, \quad (40a)$$

$$C_n^{(t)} \triangleq \frac{3}{2L_n} \left(\beta_{n,1} \left(\frac{2r_n}{1-r_n} \right)^2 + \Psi_n^{(t)} \right), \quad (40b)$$

where $r_n = \sqrt{(d_n - k_n)/d_n} < 1$ with k_n defined above (11), and the function $\Psi_n^{(t)}$ for each task n is defined by

$$\begin{aligned} \Psi_n^{(t)} &\triangleq \sum_{m=1}^M \left(v_{nm}^{(t)} - \zeta_n^{(t)} \sqrt{\gamma_n^{(t)}} |h_m^{(t)} \alpha_m^{(t)}| \right)^2 \\ &\quad + \sum_{m=1}^M |h_m^{(t)} \alpha_m^{(t)}|^2 \zeta_n^{(t)2} \gamma_n^{(t)} v_n^{*(t)}, \end{aligned} \quad (41)$$

where $h_m^{(t)}$ is the channel gain from device m defined in (8), $v_{nm}^{(t)}$ is defined in (13), $\gamma_n^{(t)}$ is the inter-task power allocation coefficient of task n defined in (15), $\alpha_m^{(t)}$ is the power allocation coefficient defined in (17), and $\zeta_n^{(t)}$ is a normalization scaling factor of task n defined in (19).

Proof. See Appendix A. \square

From Theorem 1, we see that $\mathbb{E}[\mathcal{L}(\boldsymbol{\Theta}^{(t)}) - \mathcal{L}(\boldsymbol{\Theta}^{(*)})]$, the expected difference between the training loss and the optimal

loss at the t -th round, is upper bounded by the right-hand side of the inequality in (39). Moreover, this upper bound converges with speed $\max_n \Upsilon_n$ when $\max_n \Upsilon_n < 1$. Empirically, we find that the proposed OA-FMTL scheme always converges with appropriately chosen system parameters. The following corollary further characterizes the convergence behavior of $\mathbb{E}[\mathcal{L}(\boldsymbol{\Theta}^{(t+1)}) - \mathcal{L}(\boldsymbol{\Theta}^{(*)})]$.

Corollary 1. Suppose that Assumptions 1-4 hold, and that $\max_n \Upsilon_n < 1$ for $\forall n$. Then, as $t \rightarrow \infty$, we have

$$\lim_{t \rightarrow \infty} \mathbb{E}[\mathcal{L}(\boldsymbol{\Theta}^{(t+1)}) - \mathcal{L}(\boldsymbol{\Theta}^{(*)})] \leq \sum_{t'=1}^t \sum_{n=1}^N C_n^{(t')} \quad (42)$$

Proof. When $\max_n \Upsilon_n < 1$, we have $\lim_{t \rightarrow \infty} (\max_n \Upsilon_n)^t = 0$. Plugging this result and the assumption into (39), we obtain (42). \square

Corollary 1 shows that OA-FMTL guarantees to converge with a sufficiently small $\max_n \Upsilon_n$. However, there generally exists a gap between the converged loss $\lim_{t \rightarrow \infty} \mathbb{E}[\mathcal{L}(\boldsymbol{\Theta}^{(t+1)})]$ and the optimal one $\mathbb{E}[\mathcal{L}(\boldsymbol{\Theta}^{(*)})]$ because of the communication noise and the inter-task interference. Therefore, we next aim to minimize the gap, so as to optimize our proposed framework.

V. OPTIMIZATION

A. Problem Formulation

From Theorem 1 and Corollary 1, we see that the term $\sum_{t'=1}^t \sum_{n=1}^N C_n^{(t')}$ in (42) represents the impact of the misalignment error and the estimation error caused by M-Turbo-CS on the convergence rate and the asymptotic learning performance. Specifically, a smaller $\sum_{t'=1}^t \sum_{n=1}^N C_n^{(t')}$ leads to faster convergence and a smaller gap in $\lim_{t \rightarrow \infty} \mathbb{E}[\mathcal{L}(\boldsymbol{\Theta}^{(t+1)}) - \mathcal{L}(\boldsymbol{\Theta}^{(*)})]$. This motivates us to use $\sum_{t'=1}^t \sum_{n=1}^N C_n^{(t')}$ as the metric of the FL performance, i.e., to minimize $\sum_{n=1}^N C_n^{(t)}$ over $\{\{\gamma_n^{(t)}\}_{n=1}^N, \{\zeta_n^{(t)}\}_{n=1}^N\}$ at each round t . We drop out the round index t in the following for brevity, and formulate the design problem as

$$\mathcal{P}_1 : \min_{\{\zeta_n, \gamma_n\}_{n=1}^N} \sum_{n=1}^N \sum_{m=1}^M (v_{nm} - \zeta_n \sqrt{\gamma_n} |h_m \alpha_m|)^2 \quad (43a)$$

$$\begin{aligned} &+ \sum_{n=1}^N \sum_{m=1}^M |h_m \alpha_m|^2 \zeta_n^2 \gamma_n v_n^*(\gamma_1, \dots, \gamma_N), \\ \text{s.t. } &\gamma_n > 0, \quad \forall n \in [N], \end{aligned} \quad (43b)$$

$$\sum_{n=1}^N \gamma_n \leq 1, \quad (43c)$$

where each v_n^* , which is in general a function of $\{\gamma_n\}_{n=1}^N$, is the fixed point of the state evolution in (29) and (31). In problem \mathcal{P}_1 , the objective function (43a) is equivalent to $\sum_{n=1}^N C_n$ in (40) by dropping the term irrelevant to $\{\{\gamma_n\}_{n=1}^N, \{\zeta_n\}_{n=1}^N\}$; the constraint (43c) is obtained by substituting (13)-(17) into the power constraint (9).

It is difficult to solve Problem \mathcal{P}_1 directly since the fixed point $\{v_n^*\}_{n=1}^N$ of the state evolution in (29) and (31) does not have a closed-form expression. To simplify the problem, we introduce a constraint $v_n^*(\gamma_1, \dots, \gamma_N) \leq v_n^{\text{target}}$, $\forall n$, with

v_n^{target} being a slack variable satisfying $0 \leq v_n^{\text{target}} \leq 1$, yielding a modified problem as

$$\mathcal{P}_2 : \min_{\{\zeta_n, \gamma_n, v_n^{\text{target}}\}_{n=1}^N} \sum_{n=1}^N \sum_{m=1}^M (v_{nm} - \zeta_n \sqrt{\gamma_n} |h_m \alpha_m|)^2 + \sum_{n=1}^N \sum_{m=1}^M |h_m \alpha_m|^2 \zeta_n^2 \gamma_n v_n^{\text{target}}, \quad (44a)$$

$$\text{s.t. } \gamma_n > 0, \quad \forall n \in [N], \quad (44b)$$

$$\sum_{n=1}^N \gamma_n \leq 1, \quad (44c)$$

$$v_n^*(\gamma_1, \dots, \gamma_N) \leq v_n^{\text{target}}, \quad \forall n \in [N], \quad (44d)$$

$$0 \leq v_n^{\text{target}} \leq 1. \quad (44e)$$

By inspection, it is not difficult to see that \mathcal{P}_2 has the same solution as \mathcal{P}_1 . However, the fixed point $\{v_n^*\}_{n=1}^N$ in the constraint (44d) still does not have a closed-form expression. We next give an approximate but explicit expression of the constraint (44d). To this end, we first define a simplified state transfer function as

$$z_n = \hat{\phi}_n(v_n; \gamma_1, \dots, \gamma_N), \quad \forall n \in [N], \quad (45)$$

where the function $\hat{\phi}_n$, only mapping v_n into z_n , is a simplified version of ϕ_n defined in (29). Assume that $c_1 v_1 = \dots = c_N v_N$ in (29) with predetermined constants $\{c_n | c_n \in \mathbb{R}^+\}_{n=1}^N$. The expression of the function $\hat{\phi}_n$ is given by

$$\hat{\phi}_n(v_n; \gamma_1, \dots, \gamma_N) = \left(\left(\frac{dc_n}{s\gamma_n} \sum_{n'=1}^N \frac{\gamma_{n'}}{c_{n'}} - 1 \right) v_n + \frac{d\sigma^2}{s\gamma_n} \right)^{-1}, \quad \forall n \in [N]. \quad (46)$$

The recursion in (32) and (46) continues and converges to the fixed point v_n^* for $\forall n \in [N]$, satisfying

$$\hat{\phi}_n(v_n^*; \gamma_1, \dots, \gamma_N) = \psi_n^{-1}(v_n^*), \quad (47a)$$

$$\hat{\phi}_n(v_n; \gamma_1, \dots, \gamma_N) \geq \psi_n^{-1}(v_n), \quad \forall v_n \in (v_n^*, 1], \quad (47b)$$

where $\psi_n^{-1}(\cdot)$ is the inverse of $\psi_n(\cdot)$ which exists since $\psi_n(\cdot)$ is continuous and monotonic [23]. Note that $v_n \leq 1$ since the signal power is normalized. The above recursive process is illustrated by Fig. 3. With (47a), the inequality in (44d) holds when $\hat{\phi}_n(v_n; \gamma_1, \dots, \gamma_N) \geq \psi_n^{-1}(v_n)$, where $v_n \in (v_n^{\text{target}}, 1]$ for $\forall n \in [N]$, yielding

$$\mathcal{P}_3 : \min_{\{\zeta_n, \gamma_n, v_n^{\text{target}}\}_{n=1}^N} \sum_{n=1}^N \sum_{m=1}^M (v_{nm} - \zeta_n \sqrt{\gamma_n} |h_m \alpha_m|)^2 + \sum_{n=1}^N \sum_{m=1}^M |h_m \alpha_m|^2 \zeta_n^2 \gamma_n v_n^{\text{target}}, \quad (48a)$$

$$\text{s.t. } \gamma_n > 0, \quad \forall n \in [N], \quad (48b)$$

$$\sum_{n=1}^N \gamma_n \leq 1, \quad (48c)$$

$$\hat{\phi}_n(v_n; \gamma_1, \dots, \gamma_N) \geq \psi_n^{-1}(v_n), \quad \forall v_n \in (v_n^{\text{target}}, 1], \quad \forall n \in [N], \quad (48d)$$

$$0 \leq v_n^{\text{target}} \leq 1. \quad (48e)$$

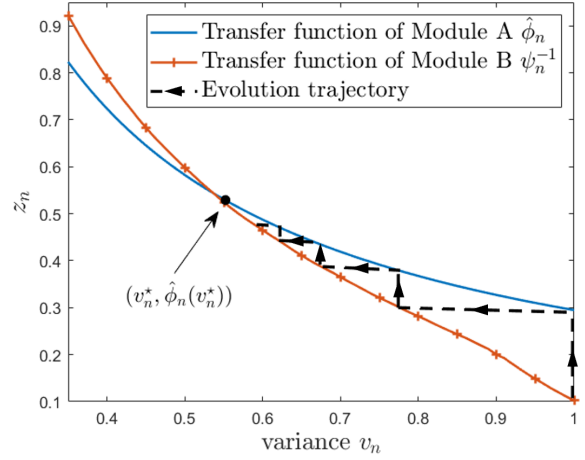


Fig. 3. An illustration of the variance transfer.

What remains is to solve \mathcal{P}_3 , as detailed in the next subsection.

B. Algorithm Design

In this subsection, we first give an equivalent form of Problem \mathcal{P}_3 . We then show that the equivalent problem \mathcal{P}_4 is readily solved by using existing optimization tools. The details are provided in the following propositions.

Proposition 1. Problem \mathcal{P}_3 is equivalent to

$$\mathcal{P}_4 : \min_{\{\gamma_n, v_n^{\text{target}}\}_{n=1}^N} \sum_{n=1}^N \left(\sum_{m=1}^M (v_{nm} - |h_m \alpha_m| \Gamma_n)^2 + \sum_{m=1}^M \left(\sqrt{v_n^{\text{target}}} |h_m \alpha_m| \Gamma_n \right)^2 \right), \quad (49a)$$

$$\text{s.t. } \gamma_n > 0, \quad \forall n \in [N], \quad (49b)$$

$$\sum_{n=1}^N \gamma_n \leq 1, \quad (49c)$$

$$\hat{\phi}_n(v_n; \gamma_1, \dots, \gamma_N) \geq \psi_n^{-1}(v_n), \quad \forall v_n \in (v_n^{\text{target}}, 1], \quad \forall n \in [N], \quad (49d)$$

$$0 \leq v_n^{\text{target}} \leq 1, \quad (49e)$$

where $\Gamma_n \in \mathbb{R}^+$ is defined as

$$\Gamma_n = \sqrt{\gamma_n} \zeta_n = \frac{\sum_{m'=1}^M v_{nm'} |h_{m'} \alpha_{m'}|}{(1 + v_n^{\text{target}}) \sum_{m'=1}^M |h_{m'} \alpha_{m'}|^2}. \quad (50)$$

Proof. For fixed $\{\gamma_n, v_n^{\text{target}}\}_{n=1}^N$, the problem \mathcal{P}_3 for finding $\{\zeta_n\}_{n=1}^N$ is a quadratic convex problem. Thus, setting the derivative of (48a) with respect to ζ_n to zero, we obtain

$$\zeta_n = \frac{\sum_{m=1}^M v_{nm} |h_m \alpha_m|}{\sqrt{\gamma_n} \sum_{m=1}^M |h_m \alpha_m|^2 (1 + v_n^{\text{target}})}, \quad \forall n \in [N]. \quad (51)$$

By plugging (51) into (48a), we obtain the objective of \mathcal{P}_4 , which completes the proof. \square

Proposition 2. For fixed $\{\gamma_n\}_{n=1}^N$, the objective function of Problem \mathcal{P}_4 is monotonically increasing with respect to v_n^{target} for each n .

Proof. For fixed $\{\gamma_n\}_{n=1}^N$, the derivative of the first term $\sum_{m=1}^M (v_{nm} - |h_m \alpha_m| \Gamma_n)^2$ in (49a) with respect to each v_n^{target} is given by

$$\frac{d \sum_{m=1}^M (v_{nm} - |h_m \alpha_m| \Gamma_n)^2}{d v_n^{\text{target}}} \quad (52a)$$

$$= \frac{d \sum_{m=1}^M (v_{nm} - |h_m \alpha_m| \Gamma_n)^2}{d \Gamma_n} \frac{d \Gamma_n}{d v_n^{\text{target}}} \quad (52b)$$

$$= \frac{2 v_n^{\text{target}}}{(1 + v_n^{\text{target}})^3} \frac{\left(\sum_{m=1}^M v_{nm} |h_m \alpha_m| \right)^2}{\sum_{m=1}^M |h_m \alpha_m|^2}, \quad (52c)$$

which is always positive. Together with the fact that $\sum_{m=1}^M \left(\sqrt{v_n^{\text{target}}} |h_m \alpha_m| \Gamma_n \right)^2$ in (49a) increases monotonically in v_n^{target} for $0 \leq v_n^{\text{target}} \leq 1$, we conclude the proof. \square

Proposition 3. For fixed $\{v_n^{\text{target}}\}_{n=1}^N$, Problem \mathcal{P}_4 for finding $\{\gamma_n\}_{n=1}^N$ reduces to a convex feasibility test problem as

$$\mathcal{P}_5 : \text{find } \{\gamma_n\}_{n=1}^N \quad (53a)$$

$$\text{s.t. } \gamma_n > 0, \quad \forall n \in [N], \quad (53b)$$

$$\sum_{n=1}^N \gamma_n \leq 1, \quad (53c)$$

$$\left(v_n + \frac{1}{\psi_{n-1}(v_n)} \right) \gamma_n - \frac{d}{s} c_n \sum_{n'=1}^N \frac{\gamma_{n'}}{c_{n'}} \geq \frac{d}{s \sigma^2},$$

$$\forall v_n \in (v_n^{\text{target}}, 1], \forall n \in [N]. \quad (53d)$$

Proof. For fixed slack variables $\{v_n^{\text{target}}\}_{n=1}^N$, the objective function (49a) is irrelevant to the optimization variables $\{\gamma_n\}_{n=1}^N$. With (46), the constraint (53d) is equivalent to (49d). Thus, Problem \mathcal{P}_4 reduces to the feasibility test in (53). Since the constraints in (53b)-(53d) are convex, Problem \mathcal{P}_5 is a convex problem. \square

Proposition 4. Suppose that for given $\{v_n^{\text{target}} = \tilde{v}_n\}_{n=1}^N$, Problem \mathcal{P}_5 is feasible. Then for any $\{v_n^{\text{target}}\}_{n=1}^N$ satisfying $v_n^{\text{target}} \geq \tilde{v}_n$, for $n = 1, \dots, N$, Problem \mathcal{P}_5 is feasible. On the contrary, suppose that for given $\{v_n^{\text{target}} = \tilde{v}_n\}_{n=1}^N$, Problem \mathcal{P}_5 is infeasible. Then for any $\{v_n^{\text{target}}\}_{n=1}^N$ satisfying $v_n^{\text{target}} \leq \tilde{v}_n$, for $n = 1, \dots, N$, Problem \mathcal{P}_5 is infeasible.

Proof. We define the feasible region of Problem \mathcal{P}_5 as $\mathcal{S}(v_1^{\text{target}}, \dots, v_N^{\text{target}})$. Based on constraints (53d), we see that for any $\{v_n^{\text{target}}\}_{n=1}^N$ satisfying $v_n^{\text{target}} \geq \tilde{v}_n$, $\mathcal{S}(v_1^{\text{target}}, \dots, v_N^{\text{target}}) \subseteq \mathcal{S}(\tilde{v}_1, \dots, \tilde{v}_N)$ holds. Similarly, for any $\{v_n^{\text{target}}\}_{n=1}^N$ satisfying $v_n^{\text{target}} \leq \tilde{v}_n$, we obtain $\mathcal{S}(v_1^{\text{target}}, \dots, v_N^{\text{target}}) \supseteq \mathcal{S}(\tilde{v}_1, \dots, \tilde{v}_N)$. Therefore, Proposition 4 holds. \square

From Propositions 1-3, to solve Problem \mathcal{P}_3 , it suffices to find the minimum values of $\{v_n^{\text{target}}\}_{n=1}^N$ such that Problem \mathcal{P}_5 is feasible. From Proposition 4, the minimum values of $\{v_n^{\text{target}}\}_{n=1}^N$ can be found by applying bisection search to each v_n^{target} . In addition, it is difficult to handle the constraint (53d) of each v_n over the entire continuous region $[v_n^{\text{target}}, 1)$. In practice, we require that (53d) holds only on some discrete points of v_n within $[v_n^{\text{target}}, 1)$. Then, the feasibility test \mathcal{P}_5 can be solved by using standard convex optimization tools. The optimization algorithm is summarized in Algorithm 2.

Algorithm 2 Optimization of OA-FMTL with M-Turbo-CS.

- 1: **Initialize** $\gamma_n = \frac{1}{N}, \zeta_n = 0, v_n^{\text{target}} = 1, \forall n \in [N]$
 - 2: Update $\{\zeta\}_{n=1}^N$ via (51)
 - 3: **for** $n = 1, 2, \dots, N$ **do**
 - 4: Use bisection search to find v_n^{target} such that Problem \mathcal{P}_5 is feasible
 - 5: **end for**
 - 6: Update $\{\gamma_n\}_{n=1}^N$ via solving Problem \mathcal{P}_5
 - 7: **Output** $\{\zeta_n, \gamma_n\}_{n=1}^N$
-

VI. NUMERICAL RESULTS

A. Experimental Settings

We validate our proposed OA-FMTL framework with experiments, and provide some baseline schemes for comparison:

- Error-free bound: This bound assumes that the ES receives all the local gradients in an error-free fashion and updates the global model by (6) and (7).
- OA-FL with TDM and Turbo-CS: Time division multiplexing (TDM) is applied to the tasks, i.e., each task is assigned with an orthogonal time slot to avoid inter-task interference. OA-FL [10] is applied in transmission, and Turbo-CS [19] is applied to recover the model aggregation at the ES.
- OA-FMTL with Turbo-CS: The proposed OA-FMTL framework is applied to transmit the model parameters of all the tasks concurrently, and the Turbo-CS algorithm is used to individually recover the model aggregation of each task by treating the inter-task interference as noise.
- OA-FMTL with M-Turbo-CS: The proposed OA-FMTL framework is applied to transmit the model parameters of all the tasks concurrently, and the M-Turbo-CS algorithm is used to recover the model aggregations of all the tasks, as outlined in Algorithm 1.

To compare the performances of the above schemes, we design two classification experiments using two commonly used databases, namely, MNIST and Human Activity Recognition (HAR). The experimental settings are as follows.

- MNIST experiment: We consider federated image classification tasks on the MNIST dataset of handwritten digits [28] and the Fashion-MNIST dataset of fashion clothing [29] (i.e., $N = 2$). For each task, we train a convolutional neural network with two 5×5 convolution layers (the first with 10 channels, the second with 20, each followed with 2×2 max pooling), a fully connected layer with 50 units and ReLu activation, and a final softmax output layer (model parameter length $d = 10920$). The learning rate is set to $\eta = 0.1$, and the compression ratio is set to $2s/d = 3/4$.
- HAR experiment: The set of data gathered from accelerometers and gyroscopes of cell phones from 30 individuals performing six different activities including lying-down, standing, walking, sitting, walking-upstairs, and walking-downstairs [30]. We first divide 30 individuals into two groups (22 cases for model training and the other 8 for model testing); and then divide the training set into four subgroups with each subgroup assigned to

an individual task classifying different human activities (i.e., $N = 4$). For each task, we train a neural network consisting of one hidden layer with the output size of 100, and the ReLU activation function, and a softmax layer for network output (model parameter length $d = 56806$). The learning rate is set to $\eta = 0.03$, and the compression ratio is set to $2s/d = 4/5$.

Other experimental settings are as follows: We consider a system of $M = 20$ local devices; the channel gain $h_m^{(t)}$ follows the Rayleigh distribution with unit variance for $\forall m \in [M]$.

B. Performance Comparisons

Fig. 4 compares the MSEs of the gradient aggregations of various schemes at $t = 90$ round in the MNIST experiment. We see that the simulation results agree well with their corresponding state evolutions. We also see that OA-FMTL with M-Turbo-CS performs better in suppressing the inter-task interference than OA-FMTL with Turbo-CS. This is expected since the latter treats the inter-task interference as noise. Besides, due to no inter-task interference in TDM, the OA-FL with TDM and Turbo-CS outperforms the others in terms of MSE. However, we will show that the learning performance of OA-FMTL with M-Turbo-CS is comparable to that of OA-FL with TDM and Turbo-CS, which reveals that OA-FMTL has a strong error-tolerance capability in gradient aggregation. Fig. 5 shows the performances of the tasks in terms of test accuracy versus communication round t . We observe that the test accuracy of OA-FMTL with M-Turbo-CS is close to that of OA-FL with TDM and Turbo-CS, and is better than that of OA-FMTL with Turbo-CS. We also note that the test accuracy of OA-FMTL with M-Turbo-CS is only about 2%-5% lower than that of the ideal error-free bound, which demonstrates the excellent interference suppression capability of OA-FMTL with M-Turbo-CS.

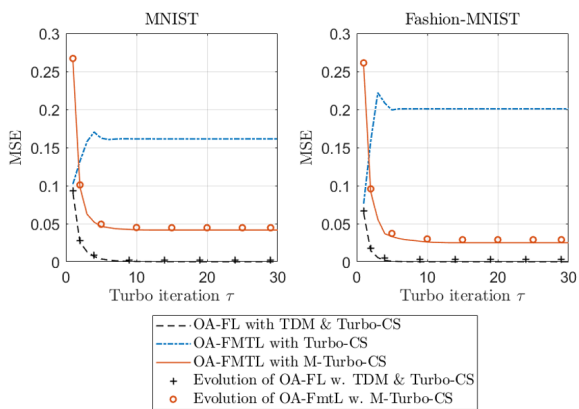


Fig. 4. The output MSE on the MNIST experiment at the communication round $t = 90$ with SNR $\frac{P_m}{\sigma_w^2} = 20$ dB, $\forall m \in [M]$.

For further comparison, we define ξ_n^{\max} as the maximum test accuracy of each task n , and define $t^*(\xi)$ as the total required rounds of communications for every task n to reach its target accuracy $\xi \xi_n^{\max}$, where ξ is called the relative target accuracy.

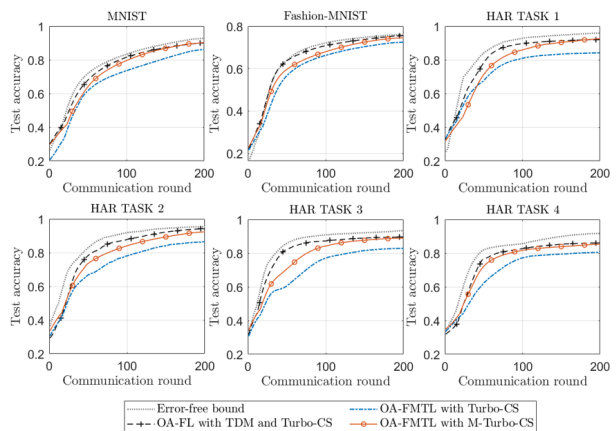


Fig. 5. The test accuracies on the two experiments with SNR $\frac{P_m}{\sigma_w^2} = 20$ dB, $\forall m \in [M]$.

Thus, $t^*(\xi)$ of the scheme including the OA-FMTL framework is given by

$$t^*(\xi) = \max\{t_1^*(\xi), \dots, t_N^*(\xi)\}, \quad (54)$$

where $t_n^*(\xi)$ is the required communication rounds of task n to reach its target accuracy $\xi \xi_n^{\max}$. Besides, $t^*(\xi)$ of the scheme with TDM is given by

$$t^*(\xi) = \sum_{n=0}^N t_n^*(\xi). \quad (55)$$

Fig. 6 depicts the total required communication rounds t^* versus relative target accuracy ξ on the two experiments. We see that OA-FMTL with M-Turbo-CS significantly outperforms the other two baseline schemes, and that the total required communication rounds of OA-FMTL with M-Turbo-CS to complete N tasks is only $1/N$ of that of OA-FL with TDM and Turbo-CS at any value of ξ . In addition, we note that OA-FMTL with Turbo-CS also requires fewer communication rounds than OA-FL with TDM and Turbo-CS, which demonstrates the advantage of non-orthogonal transmission.

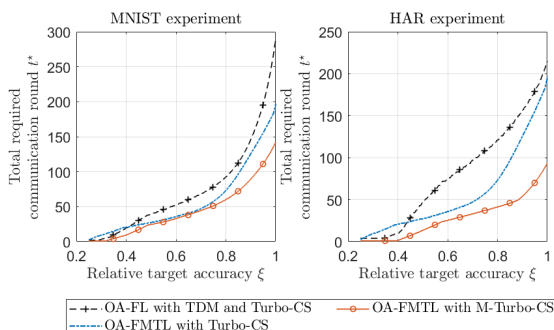


Fig. 6. (a) The required communication rounds t^* of interference-free on the MNIST experiment, with $\xi_1^{\max} = 0.78$, $\xi_2^{\max} = 0.69$ and SNR $\frac{P_m}{\sigma_w^2} = 10$ dB, $\forall m \in [M]$. (b) The required communication rounds t^* of interference-free on the HAR experiment, with $\xi_1^{\max} = 0.78$, $\xi_2^{\max} = 0.76$, $\xi_3^{\max} = 0.78$, $\xi_4^{\max} = 0.75$ and SNR $\frac{P_m}{\sigma_w^2} = 20$ dB, $\forall m \in [M]$.

We next validate the performance of the power allocation optimization for OA-FMTL with M-Turbo-CS. We describe some inter-task power allocation approaches for comparison:

- Equal power allocation: This approach assume that an equal power is allocated to each task at each communication round, i.e., we set $\gamma_1 = \dots = \gamma_N$ in Problem \mathcal{P}_1 .
- Random power allocation: This approach randomly generates the inter-task power allocation coefficients $\{\gamma_n\}_{n=1}^N$ satisfying $\sum_{n=1}^N \gamma_n = 1$.
- Optimized power allocation: This approach solves the optimization problem \mathcal{P}_3 to obtain the inter-task power allocation coefficients $\{\gamma_n^{(t)}\}_{n=1}^N$ at each communication round t .

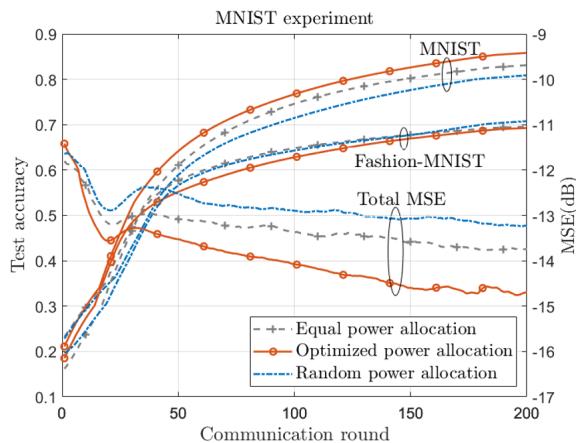


Fig. 7. The test accuracies on MNIST experiment with $\text{SNR} \frac{P_m}{\sigma_w^2} = 0 \text{ dB}, \forall m \in [M]$. Ascending curves: the performance of each task in terms of test accuracy versus communication round t . Descending curves: the total MSE, i.e., $\sum_{n=1}^N \|e_n\|^2/d$, versus communication round t .

Fig. 7 shows the performance comparison of the three power allocation approaches on the MNIST experiment and the HAR experiment, where these ascending curves measure the performance of all the tasks in terms of test accuracy versus communication round t ; and these descending curves measure the total MSE, i.e., $\sum_{n=1}^N \|e_n\|^2/d$ defined in (34), versus communication round t . Similarly, Fig. 8 shows the performance comparison of the three power allocation approaches on the HAR experiment. We see that the accuracies of some tasks are improved, e.g., MNIST, HAR TASK 2 and HAR TASK 3 at the cost of a slight decrease in the accuracies of the other tasks. We also see that optimized power allocation reduces the total MSE as compared with the other approaches. Fig. 9 depicts the total required communication rounds t^* of the three power allocation approaches on the two experiments, versus relative target accuracy ξ . We see that random power allocation significantly increases the required number of communication rounds, compared to the other allocation approaches. We also see that our proposed optimized power allocation approach reduces the required communication rounds by 25 at relative target accuracy $\xi = 1$, compared to the equal power allocation approach. This illustrates again that the optimized power allocation approach improves the overall system performance.

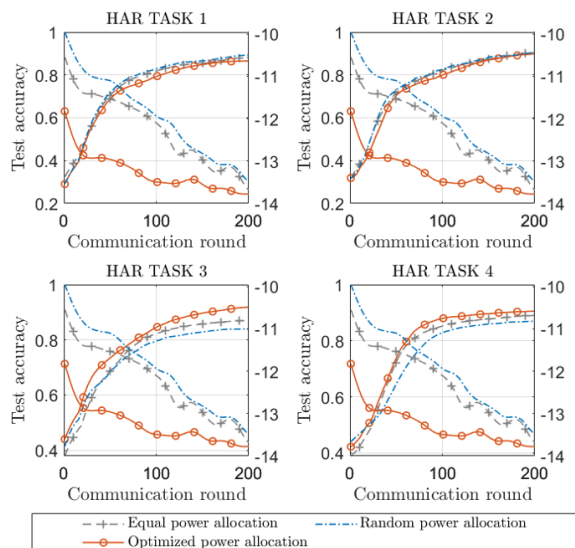


Fig. 8. The test accuracies on HAR experiment with $\text{SNR} \frac{P_m}{\sigma_w^2} = 0 \text{ dB}, \forall m \in [M]$. Ascending curves: the performance of each task in terms of test accuracy versus communication round t . Descending curves: the total MSE, i.e., $\sum_{n=1}^N \|e_n\|^2/d$, versus communication round t .

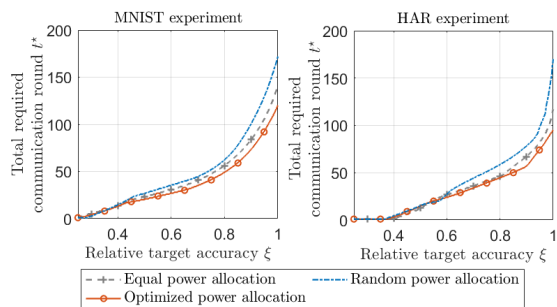


Fig. 9. (a) The required communication rounds t^* of the three power allocation approaches on the MNIST experiment, with $\xi_1^{\max} = 0.79, \xi_2^{\max} = 0.65$ and the signal-to-noise ratio $\frac{P_m}{\sigma_w^2} = 0 \text{ dB}$. (b) The required communication rounds t^* of the three power allocation approaches on the HAR experiment, with $\xi_1^{\max} = 0.86, \xi_2^{\max} = 0.86, \xi_3^{\max} = 0.83, \xi_4^{\max} = 0.83$ and the signal-to-noise ratio $\frac{P_m}{\sigma_w^2} = 0 \text{ dB}$.

VII. CONCLUSIONS

We proposed the over-the-air FMTL (OA-FMTL) framework to achieve communication-efficient FMTL in the presence of inter-task interference. Specifically, we modified the original Turbo-CS algorithm in the compressed sensing context to reconstruct the sparsified model aggregation updates at ES. We further analyzed the performance of the proposed OA-FMTL framework together with the M-Turbo-CS algorithm. Based on that, we formulated a communication-learning optimization problem to improve the system performance by adjusting the power allocation between multiple tasks on the edge devices. We showed that, under mild conditions, the problem can be solved by a feasibility test together with bisection search. Numerical simulations showed that our proposed OA-FMTL can efficiently suppress the inter-task interference, so as to achieve a learning performance comparable to its counterpart with orthogonal multi-task transmission. Mean-

while, simulations also showed that our proposed optimization algorithm further reduces the communication overhead by appropriately adjusting the power allocation among the tasks.

APPENDIX A
PROOF OF THEOREM 1

To start with, we bound $\|e_{n,1}^{(t)}\|^2$ as

$$\begin{aligned} \|e_{n,1}^{(t)}\|^2 &\leq \left(\frac{2r_n - r_n^t - r_n^{t+1}}{1 - r_n} \right)^2 \\ &\quad \times \left(\beta_{n,1} + \beta_{n,2} \left\| \nabla_n \mathcal{L}_n(\theta_n^{(t)}) \right\|^2 \right) \\ &\leq \left(\frac{2r_n}{1 - r_n} \right)^2 \left(\beta_{n,1} + \beta_{n,2} \left\| \nabla_n \mathcal{L}_n(\theta_n^{(t)}) \right\|^2 \right), \end{aligned} \quad (56)$$

where the first inequality is from [10, Appendix A], the second inequality is the upper bound obtained by making t tend to infinity, $r_n = \sqrt{(d - k_n)/d} < 1$ with k_n defined above (11), r_n^t denotes the t -th power of r_n ; and $\beta_{n,1}$, $\beta_{n,2}$ are both constants defined in Assumption 4. Then, by plugging (13) and the definition of $\mathbf{g}_n^{(t)}$ in (18) into (34), we have

$$\mathbb{E}[\|e_{n,2}^{(t)}\|^2] = \mathbb{E} \left[\left\| \sum_{m=1}^M \mathbf{g}_{nm}^{\text{no}(t)} (v_{nm}^{(t)} - \zeta_n^{(t)} \sqrt{\gamma_n^{(t)}} h_m^{(t)} \alpha_m^{(t)}) \right\|^2 \right], \quad (57)$$

where $v_{nm}^{(t)}$ is defined in (13), $\zeta_n^{(t)}$ is the normalization scaling factor of task n in (19), $\gamma_n^{(t)}$ is the inter-task power allocation coefficient of task n in (15), $\alpha_m^{(t)}$ is the power allocation coefficient of device m in (17), and $h_m^{(t)}$ is the channel coefficient of device m in (8). Then,

$$\mathbb{E}[\|e_{n,2}^{(t)}\|^2] = \sum_{m=1}^M \left(v_{nm}^{(t)} - \zeta_n^{(t)} \sqrt{\gamma_n^{(t)}} h_m^{(t)} \alpha_m^{(t)} \right)^2. \quad (58)$$

Combing (36) and (38), we obtain

$$\begin{aligned} &\mathbb{E}[\mathcal{L}_n(\theta_n^{(t+1)})] - \mathbb{E}[\mathcal{L}_n(\theta_n^{(t)})] \\ &\leq \frac{1}{2L_n} \left(3 \left(\|e_{n,1}^{(t)}\|^2 + \mathbb{E}[\|e_{n,2}^{(t)}\|^2] + \mathbb{E}[\|e_{n,3}^{(t)}\|^2] \right) \right. \\ &\quad \left. - \mathbb{E}[\|\nabla_n \mathcal{L}_n(\theta_n^{(t)})\|^2] \right). \end{aligned} \quad (59)$$

Plugging (37), (56), and (58) into (59) at the t -th training round, we have

$$\begin{aligned} &\mathbb{E}[\mathcal{L}_n(\theta_n^{(t+1)})] - \mathbb{E}[\mathcal{L}_n(\theta_n^{(t)})] \\ &\leq C_n^{(t)} - \frac{\|\nabla_n \mathcal{L}_n(\theta_n^{(t)})\|^2}{2L_n} \left(1 - 3\beta_{n,2} \left(\frac{2r_n}{1 - r_n} \right)^2 \right), \end{aligned} \quad (60)$$

where $C_n^{(t)}$ is defined in (40). Then, from [27, eq. (2.4)], we have

$$\mathbb{E}[\|\nabla \mathcal{L}_n(\theta_n^{(t)})\|^2] \geq 2\Omega_n (\mathbb{E}[\mathcal{L}_n(\theta_n^{(t)})] - \mathbb{E}[\mathcal{L}_n(\theta_n^{(*)})]). \quad (61)$$

Subtracting $\mathcal{L}_n(\theta_n^{(*)})$ on both sides of (60) and plugging (61) into (60), we obtain

$$\begin{aligned} &\mathbb{E}[\mathcal{L}_n(\theta_n^{(t+1)})] - \mathbb{E}[\mathcal{L}_n(\theta_n^{(t)})] \\ &\leq \left(\mathbb{E}[\mathcal{L}_n(\theta_n^{(t)})] - \mathbb{E}[\mathcal{L}_n(\theta_n^{(*)})] \right) \Upsilon_n + C_n^{(t)}, \end{aligned} \quad (62)$$

where Υ_n is defined in (40). Combining (62) with (2), we obtain

$$\begin{aligned} &\mathbb{E}[\mathcal{L}(\Theta^{(t+1)})] - \mathbb{E}[\mathcal{L}(\Theta^{(t)})] \\ &\leq \left(\mathbb{E}[\mathcal{L}(\Theta^{(t)})] - \mathbb{E}[\mathcal{L}(\Theta^{(*)})] \right) \max_n \Upsilon_n + \sum_{n=1}^N C_n^{(t)}. \end{aligned} \quad (63)$$

Applying the above inequality recursively yields (39), which completes the proof.

REFERENCES

- [1] K. He, X. Zhang, S. Ren, and J. Sun, "Deep residual learning for image recognition," in *Proc. IEEE Comput. Soc. Conf. Comput. Vision. Pattern. Recognit.*, Las Vegas, United states, 2016, pp. 770–778.
- [2] T. Young, D. Hazarika, S. Poria, and E. Cambria, "Recent trends in deep learning based natural language processing," *IEEE Computat. Intell. Mag.*, vol. 13, no. 3, pp. 55–75, 2018.
- [3] J. Goetz, K. Malik, D. Bui, S. Moon, H. Liu, and A. Kumar, "Active federated learning," *arXiv preprint arXiv:1909.12641*, 2019.
- [4] E. b. P. Kairouz and H. B. McMahan, "Advances and open problems in federated learning," *Found. Trends Mach. Learn.*, vol. 14, no. 1, 2021.
- [5] Y. Lin, S. Han, H. Mao, Y. Wang, and W. J. Dally, "Deep gradient compression: Reducing the communication bandwidth for distributed training," *arXiv preprint arXiv:1712.01887*, 2020.
- [6] J. Wangni, J. Wang, J. Liu, and T. Zhang, "Gradient sparsification for communication-efficient distributed optimization," in *Adv. neural inf. proces. syst.*, vol. 31, Montreal, Canada, 2018.
- [7] F. Sattler, S. Wiedemann, K.-R. Müller, and W. Samek, "Sparse binary compression: Towards distributed deep learning with minimal communication," in *Proc. Int. Joint Conf. Neural Networks*, Budapest, Hungary, 2019, pp. 1–8.
- [8] J. Konečný, H. B. McMahan, F. X. Yu, P. Richtárik, A. T. Suresh, and D. Bacon, "Federated learning: Strategies for improving communication efficiency," *arXiv preprint arXiv:1610.05492*, 2017.
- [9] G. Zhu, Y. Wang, and K. Huang, "Broadband analog aggregation for low-latency federated edge learning," *arXiv preprint arXiv:1812.11494*, 2020.
- [10] M. Amiri and D. Gündüz, "Machine learning at the wireless edge: Distributed stochastic gradient descent over-the-air," *IEEE Trans. Signal Process.*, vol. 68, pp. 2155–2169, 2020.
- [11] M. Amiri and D. Gündüz, "Federated learning over wireless fading channels," *IEEE Trans. Wirel. Commun.*, vol. 19, no. 5, pp. 3546–3557, 2020.
- [12] T. Li, A. K. Sahu, A. Talwalkar, and V. Smith, "Federated learning: Challenges, methods, and future directions," *IEEE Signal Process. Mag.*, vol. 37, no. 3, pp. 50–60, 2020.
- [13] V. Smith, C.-K. Chiang, M. Sanjabi, and A. Talwalkar, "Federated multi-task learning," *arXiv preprint arXiv:1705.10467*, 2018.
- [14] Y. Zhang and Q. Yang, "A survey on multi-task learning," *IEEE Trans. Knowl. Data Eng.*, pp. 1–1, 2021.
- [15] A. Kumar and H. Daumé, "Learning task grouping and overlap in multi-task learning," in *Proc. Int. Conf. Mach. Learn.*, Edinburgh, United kingdom, 2012, pp. 1723–1730.
- [16] C. T. Dinh, T. T. Vu, N. H. Tran, M. N. Dao, and H. Zhang, "FedU: A unified framework for federated multi-task learning with Laplacian regularization," *arXiv preprint arXiv:2102.07148*, 2021.
- [17] C. T. Dinh, N. H. Tran, and T. D. Nguyen, "Personalized Federated learning with Moreau envelopes," *arXiv preprint arXiv:2006.08848*, 2021.
- [18] T. Li, S. Hu, A. Beirami, and V. Smith, "Ditto: Fair and robust federated learning through personalization," in *Proc. Int. Conf. Mach. Learn.*, 2021, pp. 6357–6368.
- [19] J. Ma, X. Yuan, and L. Ping, "Turbo compressed sensing with partial DFT sensing matrix," *IEEE Signal Process. Lett.*, vol. 22, no. 2, pp. 158–161, 2014.
- [20] Y. Zhang and D.-Y. Yeung, "A convex formulation for learning task relationships in multi-task learning," *arXiv preprint arXiv:1203.3536*, 2012.
- [21] H. Liu, X. Yuan, and Y.-J. A. Zhang, "Reconfigurable intelligent surface enabled federated learning: A unified communication-learning design approach," *arXiv preprint arXiv:2011.10282*, 2021.

- [22] F. Seide, H. Fu, J. Droppo, G. Li, and D. Yu, "1-bit stochastic gradient descent and its application to data-parallel distributed training of speech DNNs," in *Proc. Annu. Conf. Int. Speech. Commun. Assoc.*, Singapore, Singapore, 2014, pp. 1058–1062.
- [23] J. Ma, X. Yuan, and L. Ping, "On the performance of turbo signal recovery with partial DFT sensing matrices," *IEEE Signal Process. Lett.*, vol. 22, no. 10, pp. 1580–1584, 2015.
- [24] C. Zhong, H. Yang, and X. Yuan, "Over-the-air multi-task federated learning over MIMO interference channel," *arXiv preprint arXiv:2112.13603*, 2021.
- [25] J. P. Vila and P. Schniter, "Expectation-maximization Gaussian-mixture approximate message passing," *IEEE Trans. Signal Process.*, vol. 61, no. 19, pp. 4658–4672, 2013.
- [26] K. Steven, *Fundamentals of Statistical Signal Processing: Estimation Theory*, NJ: Prentice-Hall PTR, 1993.
- [27] M. P. Friedlander and M. Schmidt, "Hybrid deterministic-stochastic methods for data fitting," *Siam J. Sci. Comput.*, vol. 34, no. 3, pp. A1380–A1405, 2012.
- [28] L. Yann, C. Corinna, and B. Christopher, "The MNIST database of handwritten digits," 1998. [Online]. Available: <http://yann.lecun.com/exdb/mnist/>
- [29] H. Xiao, K. Rasul, and R. Vollgraf, "Fashion-MNIST: A novel image dataset for benchmarking machine learning algorithms," *arXiv preprint arXiv:1708.07747*, 2017.
- [30] D. Anguita, A. Ghio, L. Oneto, X. Parra, and J. L. Reyesortiz, "A public domain dataset for human activity recognition using smartphones," in *Comput. Intell. Mach. Learn.*, Bruges, Belgium, 2013.